Journal of Computer-Aided Molecular Design, 1 (1987) 291–311
ESCOM

J-CAMD 023

Brownian dynamics simulation of protein association

Scott H. Northrup*, J. Alan Luton, Jeffrey O. Boles and John C.L. Reynolds

Department of Chemistry, Tennessee Technological University, Cookeville, TN 38505, U.S.A.

Key words: Protein electrostatics; Electron transfer; Heme proteins; Brownian dynamics; Diffusion-controlled reactions

SUMMARY

The Brownian Dynamics (BD) method is applied to study the diffusive dynamics and interaction of two proteins, cytochrome c (CYTC) and cytochrome c peroxidase (CYP). We examine the role of protein electrostatic charge distribution in the facilitation of protein-protein docking prior to the electron transfer step, assessing the influence of individual charged amino acid residues. Accurate interaction potentials are computed by iterating the linearized Poisson-Boltzmann (PB) equation around the larger protein CYP. The low dielectric constant inside proteins, electrolyte screening effects and irregular protein surface topography are taken into account. We observe a large ensemble of electrostatically stable encounter complexes seemingly with acceptable geometric requirements for electron transfer rather than a single dominant complex. Stabilities of the large variety of docking complexes are rationalized in terms of generalized charged residue complementarities. However, it is found that the electrostatic interactions giving rise to complex stabilities are somewhat nonspecific in nature. A large series of additional simulations are performed in which individual charged residues on CYTC have been chemically modified. Resulting perturbations of the association rate are significant and qualitatively similar to results observed in comparable kinetics experiments. We therefore demonstrate the potential of the Brownian dynamics method to estimate the effects of site-directed mutagenesis on protein-protein and protein-ligand diffusional association rates.

I. INTRODUCTION

The electrostatic charge distribution on the cytochromes is understood to play a crucial role in facilitating the electron transfer between these proteins in the physiological electron transport chain [1], with the electrostatic forces exerting torques which selectively steer the proteins into favorable docking arrangements [2,3]. Here we assess the role played by individual charged amino acid residues in the rate of diffusion controlled association of electron transport proteins horse heart ferrocytochrome c (CYTC) and yeast cytochrome c peroxidase (CYP). This is accomplished by performing Brownian Dynamics (BD) computer simulation of their translational and rotational diffusive motion in a highly realistic model of the protein structure and electrostatics. An extensive analysis of the electrostatic contacts involved in stabilizing complexes, and Brownian simulations

*To whom correspondence should be addressed.

of a series of modified charged amino acid residues has allowed a quantitative assessment of their relative roles.

The association kinetics of CYTC and CYP have been extensively studied experimentally [4], including a chemical modification study in which important charged lysine residues on CYTC have been selectively derivatized to a carboxydinitrophenyl (CDNP) derivative and the perturbation to the rate has been measured. We have performed simulations with comparable modifications here, offering us a unique opportunity to understand the relationship between CYTC structural features and its electron transport capabilities in particular, and to assess the role of electrostatic effects in the diffusion controlled reactions of biomolecules in a more quantitative fashion in general. Furthermore, this study establishes the usefulness of the BD methodology in making reasonable predictions of effects of site-directed mutagenesis or selective chemical modification of proteins.

In BD, the Brownian motion of interacting macromolecules is simulated stochastically by a series of small displacements chosen from a distribution which is equivalent to the short time solution of the diffusion equation [5–7]. Diffusion-influenced bimolecular reaction rate constants may then be extracted from collision probabilities calculated from a large number of BD trajectories [8–11]. The BD method has been successfully applied not only to models of the cytochromes by Northrup et al. [2,3] but to calculations of the electrostatic effects in the diffusion-controlled reaction of the enzyme superoxide dismutase (SOD) with its substrate O_2^- [12–17]. These studies have treated the irregular topography of the protein surface and have employed an iterated PB solution for the force field [17–19]. In all of the SOD and cytochrome studies, the electrostatic forces are shown to play a central role in facilitating the diffusional reaction by exerting steering forces which preorient mutual reaction partners for successful reaction.

In this paper, we provide an overview of computational work performed on the CYTC-CYP association reaction. In Section II, we describe the Poisson-Boltzmann finite difference numerical procedure used to obtain accurate interprotein interaction potentials, and the BD simulation method itself. In Section III, we present (i) results for the association rate and electrostatic details of the native protein reaction; (ii) results of the charged amino acid contacts analysis; (iii) the chemical modification study of the rates; and (iv) the effects of further improvements of the electrostatic treatment for protein-protein potentials of interaction. In Section IV, we conclude with a summary.

II. MODELS AND PROCEDURE

A. Electrostatic Potential Calculation

The electrostatic charge distribution of the proteins CYTC and CYP were derived as described in detail previously [2,3] from all-atom coordinate sets available through the Protein Data Bank [20]. The horse CYTC conformation was calculated by mutational extension of the 1.5 Å resolution tuna CYTC X-ray crystallographic structure [21], and 100 steps of steepest descents energy refinement were performed on the substituted side chains while holding the remainder of the structure fixed. Structures of the CDNP-monoderivatized CYTCs (lysine residues 7, 13, 22, 25, 27, 39, 60, 72, 73, 79, 86, and 87) were determined for this study by simply changing the charge of the lysine side-chain nitrogen from $+1e$ to $-1e$. In ongoing work, we are computing the modified

structure of the CDNP derivatives by simple model building onto lysine residues without energy refinement using standard organic substituent geometries, and growing the substituent in a direction outward along a vector defined by the α-carbon and side-chain nitrogen positions. The coordinates of CYP were taken from the 1.7 Å resolution X-ray crystallographic structure contributed by Finzel, Poulos and Kraut [22]. The 68 surface side-chain atoms missing from this set because of excessive motional disorder in the crystal were fitted into the structure using standard residue coordinates and steepest descents refinement was performed on these added atoms.

At a neutral pH, it is assumed that in both proteins all lysines and arginines are protonated, and the aspartic, glutamic and carboxy-terminal acid groups are dissociated [23]. Histidines and the amino-terminus are non-protonated. The heme propionate side chains in both proteins are assumed to be undissociated [24–26], although an additional simulation is performed in which the CYP heme propionates are dissociated. Partial charges were assigned to each heavy atom in the CYP protein, as before. Since the dynamic atom positions of CYTC must be retained explicitly during the simulation, as described below, we place charges on CYTC only at the 34 formally charged atom positions. Thus we are not required to compute, at each time step, the total force and torque placing over 866 atoms in the field generated by the CYP protein.

An accurate electrostatic potential field surrounding the larger protein CYP was computed by iterating finite difference solutions of the linearized Poisson-Boltzmann (PB) equation using the Warwicker-Watson method [27] as adapted by Klapper et al. [18]. The use of the PB equation solution rather than the simple Coulomb's law/Debye-Huckel treatment allows us to account for (i) the atomic-scale rough topography of both protein surfaces; (ii) the screening effect due to the ionic strength of the solvent medium and the absence of the same inside the larger CYP protein; and (iii) the discontinuity in the dielectric constant across the CYP protein surfaces. This allows one to obtain the potential energy, force, and torque when placing a test charge (representative of one of the charges of the nearby CYTC molecule) in the proximity of CYP. The CYP protein is represented as an irregularly shaped cavity of low dielectric constant ($\varepsilon = 4$) and zero ionic strength and having 2414 fixed imbedded charges in the conformation determined above. Selection of $\varepsilon = 4$ is based on the typical average estimate for protein interiors [23, 28–30]. Others [17] have used $\varepsilon = 2$, which is formally more valid when one is concerned with the potential field around a protein not responding to a field, and manifesting only electronic polarizability. Surrounding this cavity is a continuum dielectric with $\varepsilon = 78$ representative of water, and having ionic strengths of 0.1, 0.16, and 0.25m which screen the field emanating from the protein according to the Debye-Huckel model. The rigid rotating and translating array of 34 formal charges of CYTC is then allowed to interact with this precomputed and stored field, with direct forces and torques computed at each Brownian step. For a more accurate treatment of the electrostatic interaction between two proteins, one would need to include an additional low dielectric cavity representing the protein CYTC. However, one would need to iterate a PB solution for every possible mutual configuration of the two protein cavities, a monumental computational task. The details of the numerical iteration procedure for obtaining the potential are described elsewhere [3].

In our work, we first iterated a solution on a lattice of dimension $51 \times 51 \times 51$ elements having a resolution $d = 4$ Å and encompassing a region of size $(200 \text{ Å})^3$ centered on CYP. With such a large region, the boundary potential can be set to zero. Approximately 1500 iterations were performed to obtain complete convergence in single precision (8 significant figures). This required only 18 CPU hours of VAX11/780 time. Having obtained a solution on a large coarse grid, an ad-

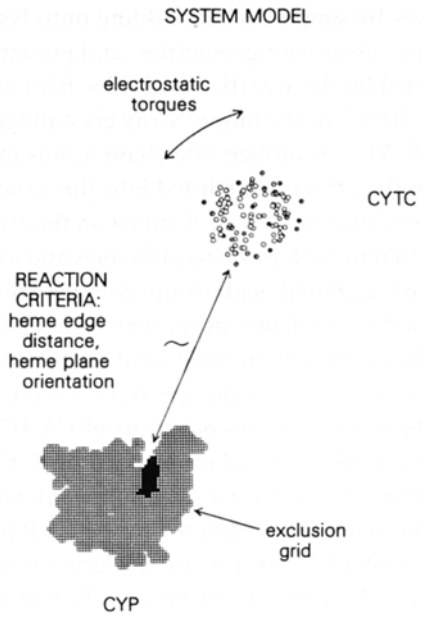

Fig. 1. Schematic picture of the detailed model system used in the Brownian simulations in which association rates of the two proteins CYTC and CYP are calculated.

ditional iteration was performed on a refined grid of resolution d = 1.666 Å of lattice size $61 \times 61 \times 61$, or a box size of $100 \times 100 \times 100$ Å. Trial solutions and boundary values for this inner lattice were constructed by interpolating the outer lattice solution. Convergence required approximately 36 hours of VAX11/780 CPU time.

B. Model System for Brownian Dynamics Simulation

We adopted a highly detailed and realistic model for the simulation of association rates of CYTC and CYP shown schematically in Fig. 1. The rough surface topography of the proteins is accounted for by developing and storing for later use in the BD simulation program a $67 \times 67 \times 67$ element cubic spatial grid of 1.0 Å resolution centered on the larger protein CYP which is used to define its excluded volume. A test atom is placed at grid points, and the distance from the test atom to each of the 2414 heavy atoms of the CYP protein is determined. If the test atom falls within 2.7 Å of any atom in the CYP protein, that grid point is defined to be in an excluded region. The test atom is representative of any one of the atoms of the partner protein CYTC diffusing into an encounter. A surface network of 105 atoms of CYTC defining its shape (including the 34 charged atoms) is tested against the exclusion grid during BD. Steps leading to overlap are omitted and repeated with new random numbers generated. The number in the set of such atoms was limited for computational efficiency, and is comprised of the 67 α-carbons beyond 11 Å from the CYTC centroid, plus all 34 formally charged atoms. This avoids having to test a large number of CYTC atoms against the CYP grid for each Brownian step. A particular shortcoming of this model is the inability of surface side chains to dynamically adjust their conformations in response to another

incoming protein, which would enhance the 'fit' of the two proteins and allow the hemes to attain a slightly closer encounter distance, as in recent studies of Mauk et al. [31]. As a result the minimum attainable heme edge distance may be inflated by as much as 3–4 Å.

A coarse lattice of dimension $51 \times 51 \times 51$ and spatial resolution of 4 Å is used to retain the PB-generated forces in a cube of width 200 Å from which interparticle forces at separations greater than 50 Å are looked up. For CYTC charges that are inside 50 Å from the origin (fixed at the center of CYP), the forces are derived from a finer grid of dimensions $61 \times 61 \times 61$ and resolution 1.666 Å. Each of the 34 charges of CYTC contribute independently to the total force and torque on the protein's rigid body motion, depending on their positions on the force grid surrounding CYP. Force vectors governing the rigid body motion of CYTC can be reduced to two vectors, one being the resultant direct force acting on the center of mass of CYTC along the line of centers between the molecules and giving rise to translational motion in relative separation space. The second vector is the resultant torque vector which influences the rotational Brownian motion of CYTC.

The relative translational motion of CYTC and CYP and the rotational motion of CYTC are thus accounted for, but the rotational motion of the larger CYP molecule is neglected in this study. In order to include its rotation, one would be required to compute the torque on CYP due to CYTC. This would entail storing the PB-generated field of force around the CYTC molecule as well, and the time-intensive looking up of forces acting on a large number of CYP charges in the PB-generated CYTC force field. In a previous study [2] using a simple spherical model with monopole/dipole forces for this same system, we determined that the neglect of the rotational motion of the CYP molecule has only a 10–20% diminishing effect on the rate constant. We hope to include CYP rotation in future studies.

The translational and rotational diffusion coefficients for each protein are assumed for simplicity to be separation-distance-independent and related to the protein hydrodynamic radius by the appropriate Stokes-Einstein relationship for spheres. Rotational and translational diffusion are assumed to be uncoupled for this simulation study.

Realistic reaction criteria are used in this study based on both the heme edge-to-edge distance d_{edge} and heme plane mutual orientation, defined by the angle ψ between heme normal vectors, which move along in rigid body motion with the protein during simulation. During the generation of a trajectory, its reactive outcome is monitored simultaneously for various possible combinations of these criteria. The distance d_{edge} is computed for each step by finding the shortest distance between one of the four CH groups bridging the pyrrole rings and the same four atoms on the other protein. Since surface side chains are not allowed to relax during protein encounter, d_{edge} is not expected to easily achieve the accepted encounter complex distance of 16.5 Å [32]. In fact, in none of the simulations did d_{edge} actually reach 15 Å. According to these criteria, we still do not discriminate between heme planes which are mutually parallel ($\psi = 0°$) and those that are also coplanar.

C. Brownian Dynamics Simulations

The basic BD trajectory simulation method [8] and its extensions [2,9,10] have been previously described. The initial protein separation for each trajectory is $b = 65$ Å between centers of mass, a spherical surface outside the region of nonnegligible electrostatic forces at these ionic strengths.

Simulation of 3000 trajectories are used to calculate p(b), the probability of reactive pair encounter for particles starting their diffusion at a distance b at randomly selected orientations. Truncation of all trajectories is performed at separation surface c = 200 Å, and an exact truncation correction is applied to p(b) as described in Ref. 8. The standard bimolecular diffusion controlled rate constant k for protein docking is then given by

$$k = 4\pi bDL\, p(b)$$

where D is the sum of translational diffusion constants, L is Avogadro's number, and p(b) is the truncation-corrected reaction probability.

The time duration of the Brownian step is determined dynamically by a procedure in which step sizes are sufficiently small to insure that forces or torques vary by $< 5\%$ over the spatial length of the step. Steps outside 134 Å are generated by an absorbing boundary algorithm for absorption of trajectories at 200Å separation. Step sizes in that region are determined so as to avoid curvature effects on the outer boundary, as previously described [10]. Table I summarizes average step sizes and numbers of steps taken in an average trajectory in three different regions of space. In an average trajectory, approximately 6300 steps (corresponding to a total of 82 ns) are taken inside a separation distance of 53 Å where forces are strong and overlap exclusions must be taken into account. Of these 6300 steps, 4500 of them are repeats due to excluded volume effects, in which case there is no necessity for recomputation of the force and torque. In the outer region (distances greater than 134 Å) where forces are negligible and step sizes are limited only by the curvature effect of the outer absorbing boundary, only 9 steps are taken in an average trajectory, accounting for an average time duration of 88 ns. In the intermediate region, where separations are between 53 and 134 Å, only 234 steps are taken per trajectory accounting for 176 ns of time. The computation time required for an average *single* BD trajectory in this problem was the equivalent of 2 min on a VAX 11/780. A single case studied here (3000 trajectories simulated for one specific mutation at a single ionic strength) required approximately 15 h of processor time on a VAX 8800 running at 1.1 million floating point operations per second, or 100 equivalent hours on the VAX 11/780. Fourteen mutations were studied, some of which were performed at various ionic strengths and

TABLE I
AVERAGE NUMBER OF STEPS AND BROWNIAN STEP SIZES TAKEN IN VARIOUS REGIONS OF SEPARATION SPACE IN A SINGLE AVERAGE BD TRAJECTORY

Region	Separation (Å)	Time step (ps)	Steps/trajectory	Duration/trajectory (ns)
total		52.5	6572	345
inner	< 53	12.9	6329	82
free	(53 134)	752	234	176
outer	> 134	9931	9	88

Central Processor Unit time requirements, in VAX11/780 equivalents
1 trajectory = 2 min
1 case (3000 trajectories at one ionic strength and one mutation) = 100 h
1 complete BD study = 3000 h

electrostatic treatment cases for an approximate total of 3000 hours of VAX 11/780 time for BD simulations alone.

In order to compare with experimental results for association rates of CYP with native CYTC gathered by Kang et al. [4], simulations were performed for binary monovalent electrolyte ionic strengths I = 0.1, 0.16, and 0.25 molal. Potential fields around CYP were computed with and without the dielectric discontinuity effect for comparison.

III. RESULTS

A. Association Rates and Electrostatic Details of the Native Proteins

The appearance of the electrostatic potential energy surface around the protein CYP in the plane of the heme (Fe at the origin of the plot) is illustrated by the contour plot given in Fig. 2. The main notable feature of the contour plot is the presence of two attractive regions (for an incoming positively charged protein surface such as that of CYTC), the most predominant of which is at the right side of the plot in a region we will refer to as Region I bounded by Asp-34, Glu-201, Glu-209, Asp-217 and Glu-290. A second more weakly attractive region we will call Region II occurs on the left side of the plot including residues Asp-217, Asp-150, Asp-146, Asp-140, and Asp-79, also in the approximate plane of the heme. These two attractive regions turn out to be two of the three regions most highly visited by the incoming CYTC molecule in the simulation in which the

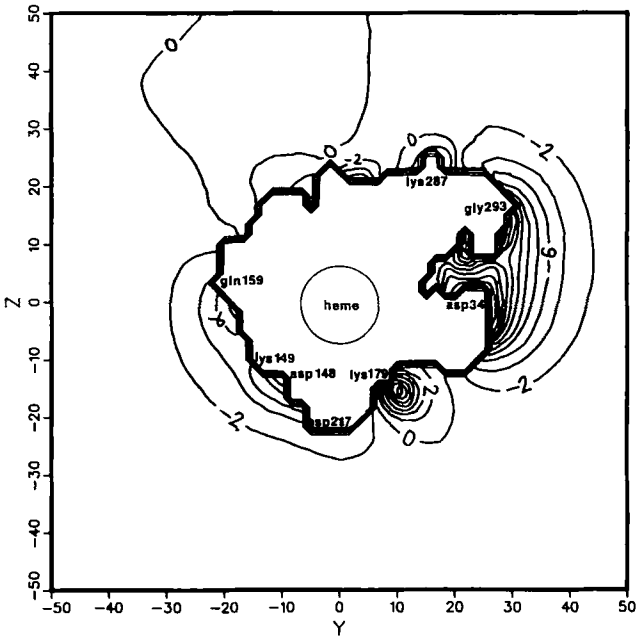

Fig. 2. Electrostatic potential energy contours in the heme plane surrounding CYP in units of k_BT, as calculated by iterating the PB equation. Values are for a +10e test charge. Cavity outlined is the region of $\varepsilon = 4$ and zero ionic strength, while the medium has $\varepsilon = 78$ and I = 0.1m.

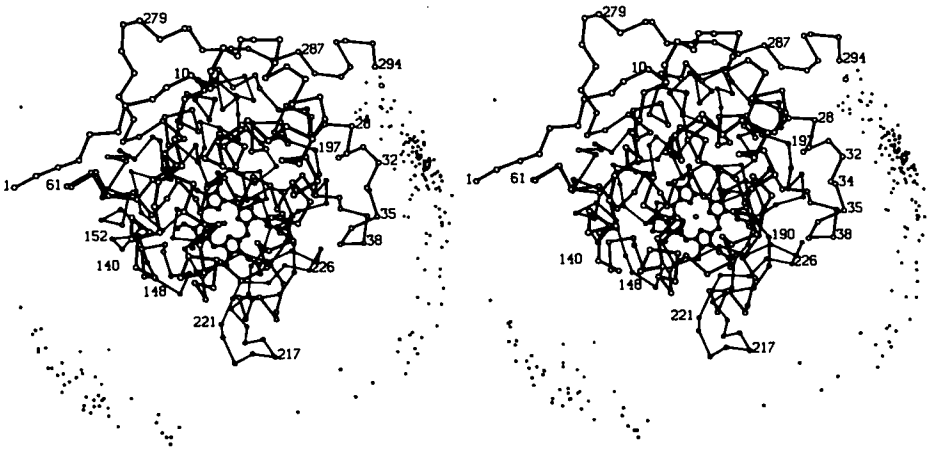

Fig. 3. Stereoscopic projection of the α-carbon skeleton and heme atoms of CYP, surrounded by points representing the center of mass of the incoming CYTC at points in space where docking criteria for electron transfer are successfully met.

very restrictive reaction criteria can be met. A third region at the bottom of the contour plot is somewhat repulsive to positive charges, in what we term here the 'Asp-217 face', including residues Asp-217, Asp-224, Glu-188, Asp-224, Glu-209, and also repulsive residues Lys-226, Lys-39, Lys-183, Lys-215, and Lys-212. This region provides a surface which is amenable to electron transfer by virtue of the proximity of the heme plane of CYP, and does contribute to the total electron transfer rate, but yet is electrostatically less favorable than the other two regions. It also occurs as a pivotal region between the other two regions, with Asp-217 showing up frequently as an important contact for both Regions I and II. In Fig. 3, we show the α-carbon skeleton and heme group of CYP oriented in the same protein orientation as the contour plot, and plot peripheral points representing the position of the center of mass of the incoming CYTC when the reaction criterion is being met. The criterion here is that $d_{edge} < 20$ Å and the heme plane orientation ψ is random. A similar picture results if heme orientation is more restricted. Notice that CYTC makes reactive approaches in two separate and primary regions, the predominant of which is near Asp-34 in the strongly attractive Region I, and to a lesser extent in the other attractive Region II near Asp-146. Both of these reactive regions occur in an equatorial belt where the CYTC center of mass approaches CYP within about 30° of the CYP heme plane. A third sparse region, the Asp-217 face, contributes weakly to the overall frequency of complexes. The hypothesized region of complex formation between CYTC and CYP as identified by Poulos and Kraut [32] is centered on Asp-34, precisely in the center of the most predominant reactive region I in Fig. 3. Our results go further in identifying the possibility and, in fact, necessity for electron transfer to occur from a range of electrostatically favorable encounter geometries. This necessity is inferred below, in that the rate constants obtained have contributions from approaches in both regions, and that an insufficient rate of association would result if association were required to take place only in one of these regions. The existence of three distinct and stable association regions for electron transfer, both of which are somewhat diffuse, as Fig. 3 illustrates, is reminiscent of the conclusion of Mauk et al. [31], whose calculations also predict the existence of an ensemble of stable protein-protein

TABLE 2
BD-SIMULATED ASSOCIATION RATE CONSTANT (x 10^{-8} $M^{-1}s^{-1}$) AT I = 0.1M FOR THE CASE OF NO COULOMBIC FORCES, AND TWO ELECTROSTATIC TREATMENT CASES A (SIMPLE COULOMBIC/POINT ION DEBYE-HUCKEL THEORY) AND C (PB NUMERICAL POTENTIAL WITH DIELECTRIC DISCONTINUITY AND EXCLUSION OF ELECTROLYTE FROM CYP PROTEIN INTERIOR.) RESULTS ARE GIVEN FOR ALL COMBINATIONS OF THE HEME COANGLE Ψ AND HEME EDGE DISTANCE CRITERIA D_{EDGE}. THE INTERPOLATED EXPERIMENTAL VALUE OF KANG ET AL. [4] FOR THIS IONIC STRENGTH IS 4.75, FOR COMPARISON

		Heme Coparallel Angle Criterion ψ		
Heme Edge Distance (Å)		30°	60°	90°
20	Zero Force	0.14	0.41	0.52
	Case A:	1.15	3.72	6.14
	Case C:	1.10	5.41	8.08
25		2.0	5.5	7.4
		8.2	16.9	21.8
		10.3	19.1	22.4
30		8.4	18.9	24.5
		19.1	32.8	38.0
		21.4	33.6	39.1

complexes rather than a single dominant stable complex that can form between CYTC and cytochrome b_5 as precursors to electron transfer.

Table 2 summarizes the results of the BD simulation study at 0.1m ionic strength showing the association rate constants as a function of heme angle requirement ψ and heme distance d_{edge} for the cases of no forces operative, simple Coulombic/point-ion Debye Huckel electrostatics (Case A) and the best electrostatic treatment (Case C). The experimental value from Kang et al. [4] interpolated to this ionic strength is 4.75×10^8 $M^{-1}s^{-1}$ for comparison. The presence of the electrostatic forces is seen to be essential to enhance the association rate into agreement with the experiment, giving an order of magnitude enhancement for the most restrictive and realistic distance criteria. Rate constants for association to $d_{edge} = 25$ Å or more give results which are significantly larger than the experimental results and are also out of line with current thinking concerning the distance effect of electron transfer. The 20 Å distance criterion which is nearest the 16.5 Å distance based on static conformational analysis [32], gives the best quantitative agreement with the experimental value when $\psi = 60°$.

In Fig. 4 we observe (at $d_{edge} = 20$ Å) that varying the heme plane requirement between 30° and 90° (the latter of which amounts to no restriction) causes a large increase in the simulated rate constant. The association rate of these proteins at random heme plane orientation is too large by about 60%, and to match experimental results we must apply the restriction of $\psi = 60°$ on heme orientation. Assuming that missing factors in our treatment will be negligible, this would support the hypothetical mechanism for electron transfer involving at least partial alignment of the heme plane advanced by numerous workers [33–35]. However, exact quantitative comparison with ex-

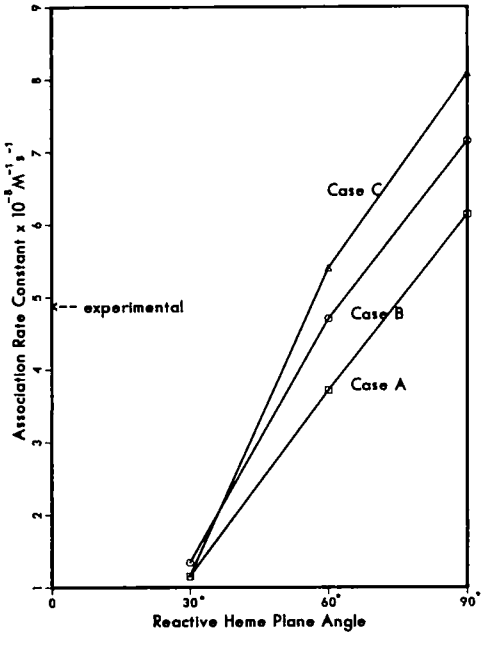

Fig. 4. BD-simulated, association rate (x 10^{-8} $M^{-1}s^{-1}$) vs. reactive heme coplanarity angle ψ at I = 0.1m for the three electrostatic treatment Cases A-C. Heme edge distance requirement is 20 Å. Experimental value is given from Ref. 4, for comparison.

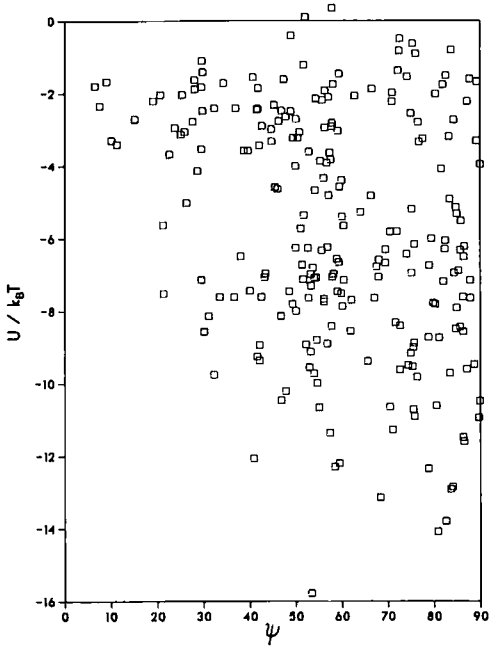

Fig. 5. Interaction potential energy of 243 complexes minimally satisfying the geometric requirements for electron transfer as a function of their heme plane alignment ψ.

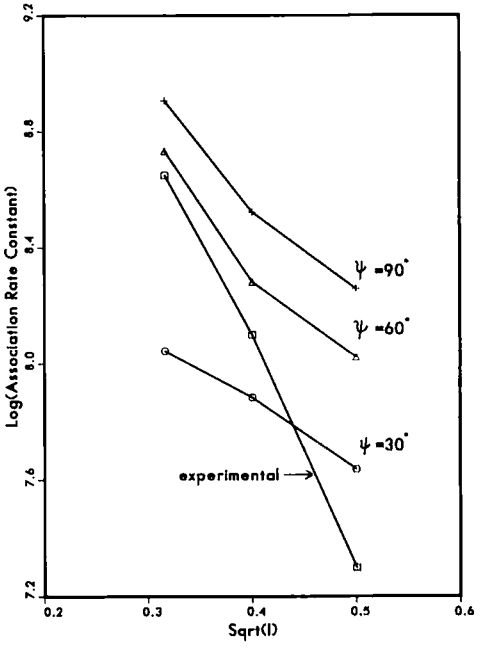

Fig. 6. Log10 of the simulated diffusion-controlled bimolecular rate constant for CYTC-CYP association vs. square root of ionic strength. Rates for three choices of heme plane orientation requirement ψ are given, at fixed d_{edge} = 20 Å. The experimental curve is from Ref. 4.

periment should be made with caution in that we are ignoring considerable, dynamical details of short-range approaches of proteins, viz., the adjustment of surface side chains for increased stabilization.

Fig. 5 also illustrates the effect of improving the treatment of solvent mediation effects by comparing Cases A, B and C. For the reaction criteria predicting nearest agreement with experiment ($d_{edge}=20$ Å, $\psi=60°$), the exclusion of the electrolyte atmosphere from penetration of the CYP protein (Case A→B) enhances k by 30%. The further inclusion of a low dielectric treatment of the CYP cavity (Case B→C) gives an additional enhancement of 15% for a combined increase of the rate of 45%. This indicates the importance of the inclusion of both of these effects in the accurate treatment of the electrostatic interactions between proteins in aqueous media at physiological ionic strength. Similar enhancement is noted at $\psi=90°$. It is surprising to note, however, that for the $\psi=30°$ case the improvement of the electrostatic treatment has a negligible effect. This may be explained by observing the average interaction potential vs. ψ of pairs reaching the proper geometry for reaction at $d_{edge}=20$ Å, as we plot in Fig. 5. Apparently because of fortuitous unfavorable electrostatic contacts in parallel heme plane encounters, the average interaction potential for $\psi=30$ encounters is attractive ($-2k_BT$), but less attractive than encounters at less restrictive heme plane orientations ($-8k_BT$). This also explains why the ionic strength dependence of the rate is less pronounced at $\psi=30°$ than at $\psi=60°$ or 90°, as we will discuss with regard to Fig. 6 below.

In Fig. 6, we observe the ionic strength dependence of the simulated and experimental association rate using the most realistic heme edge distance requirement $d_{edge}=20$ Å. Note again that agreement with experiment at three ionic strengths is obtained with the intermediate heme angle criterion $\psi=60°$. Especially note that the simulation produces good agreement in the ionic strength dependence of the rate constant in the range between I=0.1m and 0.16m (near physiological ionic strength) using $\psi=60°$. This is in contrast to the much weaker ionic strength dependence observed in the context of the simple spherical monopole/dipole electrostatic model with Coulomb's law/Debye-Huckel forces [2]. Deviation occurs at higher ionic strength, which is not surprising in that we are employing the linearized PB equation, which is expected to break down at ionic strengths much over 0.1m, and are using a continuum treatment of the electrolyte medium which neglects ion-ion correlations. The ionic strength dependence of the $\psi=30°$ case is much weaker and does not match experimental results. As shown above and also discussed in Section IIIB, fortuitous bad electrostatic contacts decrease the stabilization of complexes with the best heme plane alignment, giving rise to a flatter ionic strength dependence.

B. Amino Acid Contacts Analysis in Native Docked Complexes

During the BD simulations the configurations of the protein-protein system were saved on disk at instants in time in which geometric docking criteria were met with $d_{edge}=20$ Å. The saved center of mass positions and protein orientation reference vectors were used later to reconstruct the full atomic conformation of docked proteins. These were analyzed in a number of ways, including a tabulation of the frequency of contacts made by individual amino acid residues, frequency of electrostatic pairs formed between proteins, and frequency of diads and triads of electrostatic pairs.

Fig. 7 shows for CYTC the frequencies in which individual charged residues are among the top

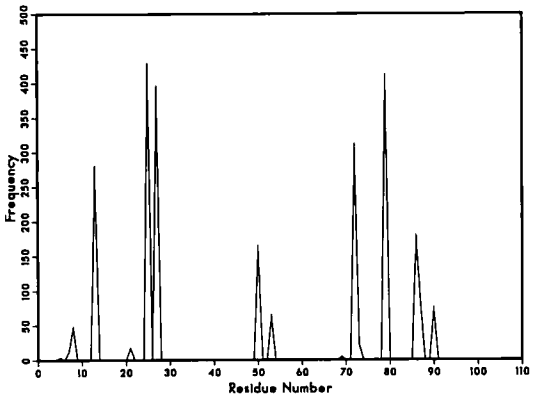

Fig. 7. Frequency at which individual charged amino acids of CYTC occur as one of the top ten closest contacts with CYP upon formation of electron transfer docked complexes.

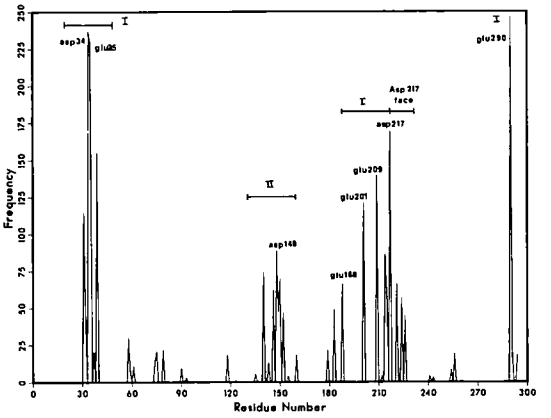

Fig. 8. Frequency at which individual charged amino acids of CYP occur as one of the top ten closest contacts with CYTC upon formation of electron transfer docked complexes. The three most frequently visited faces of CYP are indicated as Regions I, II and the 'Asp-217 Face'.

ten closest contacts in docked configurations. Lysines 13, 25, 27, 72, 79, 86, and 87 are most heavily involved in favorable electrostatic interactions with CYP. These all occur on the front face of CYTC containing the heme edge, as expected. Lysines 7, 8, and 73 make favorable contacts but to a much lesser extent. Negatively charged Asp-50, also located on the front of CYTC, makes frequent contact but of a destabilizing nature, most often with negatively charged CYP residues Glu-35 and Glu-290. In likewise manner, negatively charged CYTC residue Glu-90 makes frequent destabilizing contacts, most regularly with Glu-35 on CYP.

Fig. 8 shows for CYP the frequencies in which individual charged residues are among the top

TABLE 3
RELATIVE FREQUENCIES OF THE MOST FREQUENT ELECTROSTATIC CONTACTS OBSERVED IN DOCKED COMPLEXES OF CYTC AND CYP

	Cytochrome c residues				
CYP RESIDUES	Lys-13	Lys-25	Lys-27	Lys-72	Lys-79
Asp-34	38	55	26		40
Glu-35	55	44			26
Lys-39	30	31			28
Asp-148					30
Glu-188			32		
Glu-201			29		63
Glu-209					32
Glu-214		30			
Asp-217		28	33		
Glu-290		39	45	34	

ten closest contacts in docked configurations. Three distinct regions on the surface of CYP are represented by the residues making most frequent contact. Region I is represented by Asp-34, Glu-35, Glu-201, Glu-209 and Glu-290, all contributing to the stability of docked complexes. Region I also contains positively charged residue Lys-39 which frequently interferes with docking. Region II, which is a completely separate face allowing geometrically feasible electron transfer complexes, is stabilized by contacts involving Asp-79, 140, 146, and 150, and Glu-221, and is destabilized by Lys-149. A third region which is intermediate between Regions I and II is the 'Asp-217 face", which frequently involves stabilizing contacts from Lys-217, Glu-188, Asp-224, Glu-214, Glu-221 and destabilizing contacts from Lys-226 and Lys-183.

Table 3 shows the most frequent electrostatic contact pairs resulting in geometrically promising complexes which form between the five most prominent CYTC residues and the 10 most prominent CYP residues. The table shows results of 243 separate complexes formed in BD simulation, in each of which the ten closest contacts are identified. The number in the table represents how many of these complexes contain the corresponding contact pair. For CYTC, Lys-25 and 79 show the most versatility, making frequent contacts with most of the important CYP residues.

In order to attempt to identify a single dominant electrostatic complex between the two proteins, we analyzed the frequency of diads and triads of interprotein ion pairs in Tables 4 and 5, re-

TABLE 4
FREQUENCIES OF THE MOST FREQUENT OCCURRENCES OF TRIADS OF CONTACTS IN DOCKED COMPLEXES OF CYTC AND CYP

CYP residue	CYTC residue	Frequency
Asp-34/Glu-35	Lys-79	11
Glu-209	Lys-13	
Glu-290	Lys-25/Lys-27	
Asp-34/Glu-35	Lys-13	8
Glu-188	Lys-25/Lys-27	
Asp-217	Lys-25/Lys-27	
Glu-201	Lys-79	8
Glu-209	Lys-79	
Glu-290	Lys-72	
Asp-34/Glu-35	Lys-13	7
Glu-201	Lys-79	
Glu-209	Lys-79	
Asp-34/Glu-35	Lys-79	7
Glu-201	Lys-25/Lys-27	
Glu-290	Lys-25/Lys-27	
Asp-34/Glu-35	Lys-13	6
Glu-201	Lys-79	
Glu-290	Lys-72	
Asp-34/Glu-35	Lys-13	6
Asp-34/Glu-35	Lys-86	
Glu-201	Asp-79	

TABLE 5
FREQUENCIES OF THE MOST FREQUENT DIADS OF ELECTROSTATIC CONTACTS IN DOCKED COMPLEXES OF CYTC AND CYP

CYP residue	CYTC residue	Frequency
Asp-34/Glu-35 Glu-290	Lys-79 Lys-25/Lys-27	24
Glu-201 Glu-209	Lys-79 Lys-79	15
Asp-34/Glu-35 Glu-290	Lys-13 Lys-72	15
Asp-34/Glu-35 Glu-201	Lys-13 Lys-79	14

spectively. These data clearly show that there is no dominant complex which forms, but a surprisingly even distribution over a variety of complexes. The most frequent complex which forms (but still only 11 times out of the 243 analyzed) is the triad in which CYP residues Asp-34/Glu-35, Glu-209 and Glu-290 contact CYTC Lys-79, Lys-13 and Lys-25/27, respectively. These are Region I complexes, two typical complexes of which are plotted in Fig. 9, which we describe below.

Fig. 9–11 depict the complementarity between the contact surfaces of CYP, facing upward, and CYTC surfaces, facing downward, of four typical and representative complexes. Only the residues at the interface are shown for clarity, with CYTC residues darkened, and CYP shown by the open circles. The orientation of the heme planes are sketched also. Connections are drawn between residues which make the closest contacts. In Fig. 9 we see two complexes being made to Region I of CYP, with the CYTC orienting itself in two possible ways which are separated by a 180° rotation around the approach axis. The two complexes are approximately equally stable with $d_{edge} = 20$ Å, while ψ is almost 90° in both orientations. The heme edge face of CYTC hence consists of four corners of positive charges – Lys-25/27, Lys-79, Lys-72/86 and Lys-13/87, of which three of the four may simultaneously match up with a triangle of charges on the Region I face of CYP consisting of Asp-34/Glu-35, Glu-290, and Glu-201/209. During Brownian diffusional encounter, the proteins may sample several of these alignments simply by a rotation around the approach axis. The alignment giving parallel heme planes appears to be hindered by repulsive contacts of Asp-50 with Glu-290, contributing in part to the decreased stabilization at small values of ψ as seen in Fig. 5.

Approach of the two proteins at the Region II of CYP is shown in Fig. 10. This complex gives heme parallelity at a $d_{edge} = 20$ Å, and is stabilized by interactions of CYTC residues Lys-25 and 27 with CYP residues Asp-148, 150 and Glu-221, as well as Lys-79 with Asp-79 and 146. Between Region I and II there is an additional approach surface on CYP we call the 'Asp-217 face'. A typical complex in this region is shown in Fig. 11. This particular complex is stabilized by contacts between CYP Asp-217 and CYTC Lys-86, between CYP Asp-224 and Glu-214 and CYTC Lys-13, and between CYP Glu-188 and CYTC Lys-72, with near heme coparallelity. Although heme planar alignments appear to be made more easily in this region, the overall electrostatic potential in

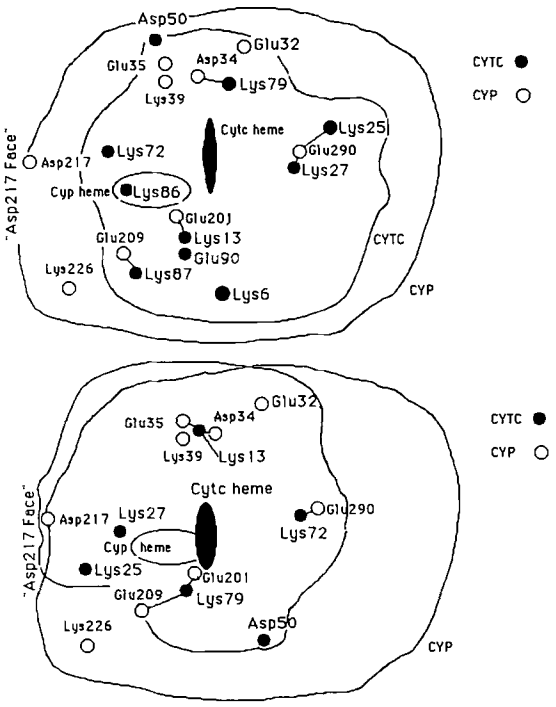

Fig. 9. An approximate cross section showing the complementarity of overlap of the interfacial region between CYTC (facing down) and CYP (facing up). The top and bottom pictures represent two approaches of CYTC to the same CYP face (Region I); the two approaches differ by a CYTC rotation of 180° around the approach axis. Closest interprotein contacts are connected by a solid line.

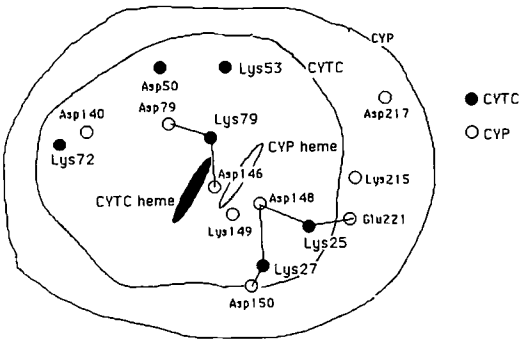

Fig. 10. An approximate cross section showing the complementarity of overlap of the interfacial region between CYTC (facing down) and CYP (facing up). This complex occurs on the Region II face of CYP. Closest interprotein contacts are connected by a solid line.

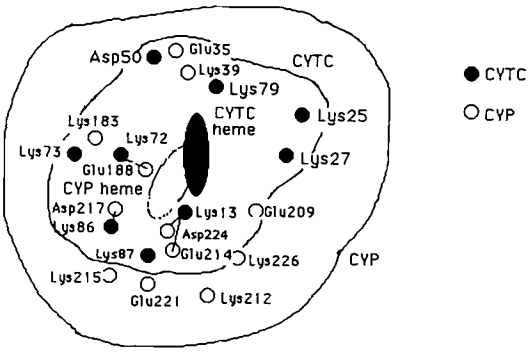

Fig. 11. An approximate cross section showing the complementarity of overlap of the interfacial region between CYTC (facing down) and CYP (facing up). This complex occurs on the Asp-217 face of CYP. Closest interprotein contacts are connected by a solid line.

this area around CYP is less attractive than Region I due to a number of positive charges including Lys-183, 212, 215, and 226. This effect can be observed in the contour plot Fig. 2.

The contact analysis of 243 complexed states revealed that their electrostatic stabilities are typically due to the interaction of 2–4 ion pairs with varying degrees of complementarity. This provides an explanation of the ionic strength dependence of the rate constant as shown in Fig. 6. Despite the large net monopole on these proteins (+8e and −12e for CYTC and CYP, respectively) the ionic strength dependence was much weaker and reflected the interaction of approximately 4e charges of opposite sign, in keeping with the finding of the contact study. This lends support to

the hypothesis that it is the net electrostatic charge in the neighborhood of the interaction domain that primarily affects the association rate ionic strength dependence, and not the global properties of the proteins.

C. Chemical Modification Studies

In order to identify the binding domain of CYTC, Kang et al. [4] have performed kinetics experiments in which various chemically modified horse CYTCs were reacted with yeast CYP and kinetic data were collected on their electron transfer capabilities. They derivatized Lys-8, 13, 25, 27, 60, 72, 73, 86, and 87 by preparing the CDNP derivative of the lysyl side chain. These modified proteins have structural and redox properties which are unchanged from the native horse CYTC. In similar fashion, we have simulated the Brownian association rate of CYP associating with this series of CDNP-modified CYTC proteins for comparison purposes, including additional simulations of modified residues Lys-7, 22, 39, and 79. In addition we have converted the $-1e$ charge of Asp-50 into $+1e$ to confirm its role as a detractor of the association process, as deduced from the contact analysis. In addition we have regenerated the Poisson-Boltzmann solution around CYP for the case in which the heme propionates on CYP *are* dissociated in order to deduce this effect on the rate. In this first series of simulations we approximated CDNP-derivatized lysines simply by changing the charge on the lysine nitrogen from $+1e$ to $-1e$ without changing its location. This ignores the steric effect of the chemical modification. In current simulations which are not yet completed, we are repeating the simulations after approximating a new location for the $-1e$ charge at a point 6.2 Å beyond the lysine nitrogen on a vector emanating from the lysine α-carbon.

TABLE 6
KINETIC RESULTS OF CHEMICAL MODIFICATION STUDIES AT 0.1m IONIC STRENGTH. COMPARISON IS MADE TO EXPERIMENTAL RESULTS OF KANG et al. [4]. BD RESULTS ARE SHOWN FOR A HEME PLANE CRITERION OF $\Psi = 60°$

Modification	BD Relative activity	Exptl Relative activity
Lys-27→ −1e	0.38	0.24
Lys-79→ −1e	0.41	–
Lys-72→ −1e	0.52	0.13
Lys-86→ −1e	0.54	0.16
Lys-13→ −1e	0.59	0.24
Lys-25→ −1e	0.64	0.57
Lys-87→ −1e	0.70	0.19
Lys- 8→ −1e	0.78	0.63
Lys-73→ −1e	0.81	0.33
Lys-60→ −1e	0.82	1.00
Lys- 7→ −1e	0.91	–
Native CYTC	1	1
Lys-22→ −1e	1.01	–
Lys-39→ −1e	1.11	–
Asp-50→ +1e	2.00	–
CYP heme propionates dissociated	1.27	–

This will allow us to make an estimate of the *steric* effect of the substitution which the experimenters were unable to make. Simulations were performed at an ionic strength of 0.1m, and results are tabulated in Table 6 in terms of both association rate constants and *relative activity*, which is defined as the ratio of the rate constant of the modified protein to that of the native protein

$$\text{Relative activity} = k_{CDNP}/k_{NATIVE}$$

In the experiment, the lowest relative activities (meaning largest detraction from the docking rate) were obtained when derivatizing Lys-72, 86, 87, 27 and 13. Only moderate effects were observed for modifications of Lys-73, 25 and 8, while no perturbation was observed for Lys-60, which is on the opposite side of CYTC from the heme edge. In our simulation studies we observed qualitatively the same kind of effects of the chemical modification series, as shown in Table 6. Modification of Lys-27, 72, 86 and 13 produced the largest retardations of the rate, just as observed experimentally, though not to the same degree. We did not observe Lys-87 to be in this group of largest perturbations, but its influence was more moderate. In the range of more moderate influences we predicted Lys-25, 8, and 73, just as the experiment showed. However, Lys-60 also showed a slight retardation of the rate in the simulation when chemically modified, while no effect was observed in the experiment. We also ran simulations of derivatized Lys-79, 7, 22, and 39, which were not performed in the experiment. Derivatization of Lys-79 showed one of the largest retardations of the rate, just as we might have expected from its significance in the contact analysis study of native protein complexation. No effects were observed by modification of Lys-7, 22, and 39. This is also to be expected, as these are located on the 'sides' of CYTC and away from the exposed heme edge region. Since Asp-50 is a prominent negative residue in the region of the heme edge and is anticipated to have a negative influence on complexation as seen in the contact study, an additional simulation was performed in which the charge of Asp-50 on CYTC was changed from $-1e$ to $+1e$, while the charge location was not changed. Just as expected, the removal of a $-1e$ charge from the predominantly positive heme edge surface of CYTC and replacement with a $+1e$ charge resulted in an improvement of the docking rate. What is surprising is that the rate actually *doubled* from the native simulations. Thus we would predict a strong evolutionary driving force for proteins to explore new site-modifications in order to enhance their effectiveness to form complexes with other proteins when electrostatic forces are involved.

In addition to modifications on the CYTC protein we also performed a charge modification on the CYP protein. Since it is not clear whether heme propionates are in a dissociated state, we regenerated the electrostatic field around CYP after having placed $-1e$ charges on each of the two heme propionic acid groups. Since these groups are oriented essentially in a direction toward the dominant complex forming region, we expect an improvement of the association rate and, in fact, we observed a 25% enhancement of the rate upon this modification (see bottom of Table 6). We cannot necessarily conclude that the dissociated state is the dominant state for CYP on this basis, since reasonably good agreement with the experiment is observed without heme propionate dissociation and there are a number of other uncertain factors, such as the correct choice of parameter ψ.

D. Further Considerations of Electrostatic Interactions of Proteins

An accurate treatment of the electrostatic interaction between folded proteins in aqueous electrolyte environments is a major consideration in the Brownian dynamics of protein association. This is of obvious importance to the molecular interactions taking place in the electron transport chain. A major shortcoming of the electrostatic model employed here is the neglect of treating the region of the smaller CYTC protein (i) as a low dielectric region, as well as a region which (ii) excludes the presence of the diffusible electrolyte ions and their Coulombic screening capability. These considerations have been neglected in the simulations in order to avoid the monstrous computational problem of reiterating the PB solution for every possible mutual configuration of the two protein cavities. Thus only the larger CYP protein is treated as a low dielectric material and one which excludes electrolyte penetration. The smaller protein is placed into the PB field of the larger protein as an array of independent test charges for the computation of total protein-protein potential energy, force and torque. This is an obvious improvement on the Debye-Huckel (DH)

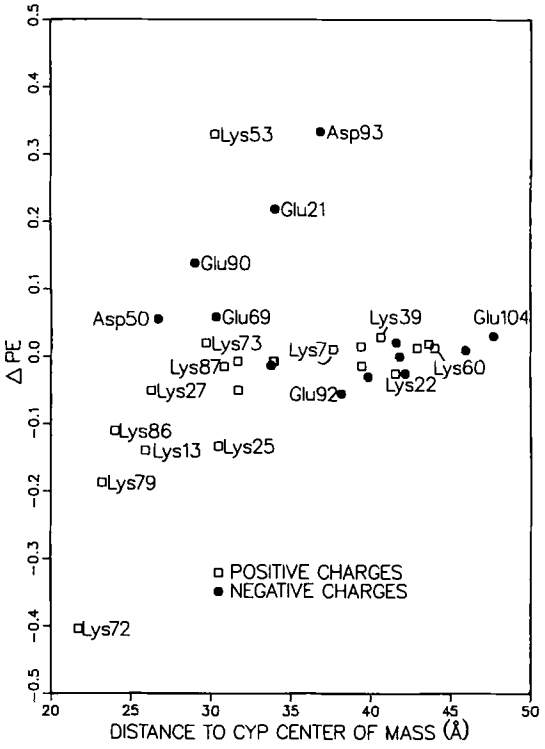

Fig. 12. The potential energy change experienced by individual charged residues of CYTC when docked in one example complex with CYP (corresponding to the configuration shown in the bottom part of Fig. 9. The change denotes the difference (in k_B T units) when properly including the low dielectric zero-ionic-strength cavity on the second protein CYTC.

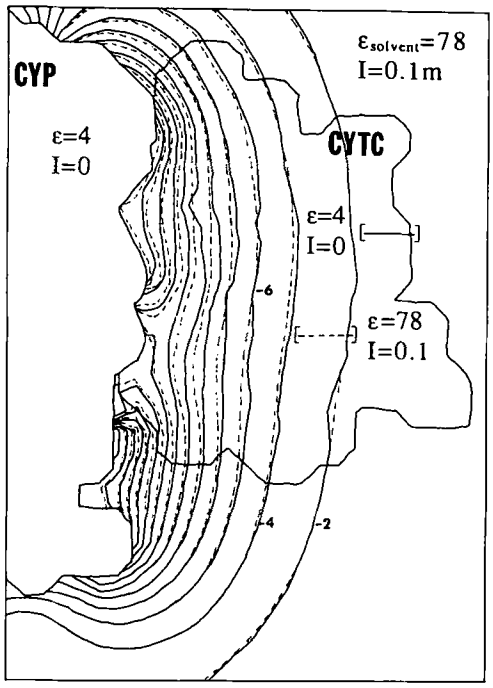

Fig. 13. Potential energy contours generated by CYP with (—) and without (---) inclusion of the second low dielectric I = 0 region inside CYTC, the protein cavity outlined on the right of the picture.

theory in which the entire space has a constant dielectric and ionic strength characteristic of the medium. In order to determine the improvement we have made in treating the CYP protein correctly and the additional influence of correctly treating the CYTC interior as well, we have done side calculations here in which we have taken three representative docked complexes discussed in the contact analysis study of Section IIIB and performed an iteration of the PB equation in which *both* protein cavities are included correctly. The potential field emanating from the full array of charges inside CYP and propagating through a chargeless CYTC cavity is derived. After convergence, the array of CYTC is placed into this field and the interprotein interaction potential is computed by treating each CYTC charge as a test charge in the CYP field. This is a completely consistent method of computing the interprotein interaction within the context of the linearized PB equation. In all three complexes, the introduction of the CYTC cavity had virtually *no effect* on the total interaction potential. The field experienced by individual CYTC charges due to CYP was modified by the inclusion of the second protein cavity, but the overall effect was cancelled. Fig. 12 shows the change in potential energy of each of the 34 CYTC formal charges in units of k_BT for one of the complexes as a function of that charge's distance from the CYP center of mass. Charges closer to the interface between proteins obviously experience a greater perturbation by inclusion of the CYTC cavity, but stabilizations and destabilizations cancel one another out in the cases studied. Fig. 13 shows for the same complex the change in the potential energy contours inside the CYTC cavity by its treating it as a low dielectric, zero ionic strength region.

In addition to the above calculation, we also examined the energetics of all 243 complexes ($d_{edge} = 20$ Å) which formed during BD simulation of the native proteins in ionic strength of 0.1m. In each of these, we compared the interprotein potential energy obtained using the simple DH continuum theory with the PB-generated potential used in the BD simulations and having the correct inclusion of one protein cavity (the CYP protein). Inclusion of the low dielectric and zero ionic strength inside CYP caused an average 30% enhancement of the electrostatic stabilization, demonstrating the degree of importance of accurate treatment of interprotein electrostatics, particularly of the larger of the two proteins (the CYP effective radius is 28 Å, compared to 18 Å for CYTC).

IV. CONCLUSION

In this paper, the BD method has been applied to calculate the diffusion-controlled association rate of electron transfer proteins cytochrome c and cytochrome c peroxidase. We have examined the role of protein electrostatic charge distribution and solvent mediation in the facilitation of protein-protein docking prior to the electron transfer step. An accurate interaction potential is computed by iterating the linearized Poisson-Boltzmann equation around the larger CYP protein, and allowing the 34 formal charges of the smaller CYTC protein to interact with this field. The discontinuity in the dielectric constant across the CYP surface and the irregular surface topography of both proteins are thus accounted for. Realistic criteria for determining the successful docking of the proteins are based on a combination of the mutual orientation of heme planes and the heme edge-to-edge distance. The proteins are found successfully to meet the most realistic distance criteria (heme-edge distance less than 20 Å) along lines of approach in three distinct regions of relative separation space. These regions are in a belt approximately in the CYP heme plane and the two major ones are found to coincide with the two electrostatically attractive regions observed

in that plane. The most predominant of these regions matches the region around Asp-34 of CYP hypothesized by Poulos and Kraut [32]. The second dominant region is substantially removed from the major region and is centered around Asp-148. A third region in the area of Asp-217 on CYP is less electrostatically attractive, but is accessible to the heme group geometrically and contributes somewhat to the overall rate of association. The existence of a large nonspecific ensemble of stable encounter complexes is consistent with the observed behavior in the similar case of CYTC and cytochrome b_5 docking [31].

The reaction criteria giving a best match to the experimentally determined association rate is the case where heme edge distance must be within 20 Å and the heme planes must be parallel to within 60°. Association at random heme plane orientation takes place at a rate which is twice as large as the experiment. It is difficult to conclude from this study, however, what are the correct geometric criteria for electron tranfer since a number of factors are missing in the simulation model, particularly the ability of the side chains to dynamically adjust their conformations to optimize electrostatic binding. Since this dominant missing factor is likely to *increase* the simulated rate under all the geometric cases considered, the implication is that the electron transfer mechanism will involve at least partial alignment of the heme planes, and probably more than we have predicted here. Whatever the case may be, the geometric requirements appear to be met through basically two surfaces (and possibly a third surface) of the CYP protein rather than from a single complexation state. From an analysis of the electrostatic contacts giving rise to these complexed states, we find that the frequency of various contacts are widely distributed, implying essentially a nonspecific binding process in which a predominantly positive surface of CYTC interacts with a predominantly negative surface of CYP. Not only is the detailed potential energy map around the CYP protein rationally consistent with the successful approach vectors for reaction observed in the simulation, but the association rate in the absence of electrostatic forces is exceedingly slow, indicating the critical necessity of at least the general features of the electrostatic distribution. The chemical modification study has produced results at least in qualitative agreement to those of the experiment, and have thereby demonstrated the feasibility of predicting the rate effect of mutations at critical positions on the protein surfaces.

Additional improvements must be made to optimize the treatment within the context of BD simulation methodology, particularly: (i) inclusion of the rotation of the larger protein (requiring an additional storage grid of forces surrounding the CYTC protein); (ii) inclusion of hydrodynamic interactions based on the irregular geometry of the proteins [36]; (iii) inclusion of a low dielectric treatment inside the smaller protein CYTC (although this is shown to perhaps not have a tremendous effect); and (iv) inclusion of the capability of mobile charged surface side chains to dynamically adjust their positions during protein-protein docking [31]. Such improvements are under consideration for future studies. For the simulation of the chemically derivatized CYTCs we expect more quantitative agreement when the structural details of these perturbations are included in a more realistic fashion.

ACKNOWLEDGEMENTS

This work has been made possible by grants DK01403 and GM34248 from the National Institutes of Health and by grant 17051-B7 from the Petroleum Research Fund as administered by the American Chemical Society. S.H.N. is the recipient of an NIH Research Career Development Award.

REFERENCES

1 Margoliash, E. and Bosshard, H.R., Trends Biochem. Sci., 8 (1983) 316–320.
2 Northrup, S.H., Reynolds, J.C.L., Miller, C.M., Forrest, K.J. and Boles, J.O., J. Am. Chem. Soc., 108 (1986) 8162–8170.
3 Northrup, S.H., Boles, J.O. and Reynolds, J.C.L., J. Phys. Chem., 91 (1987) 5991–5998.
4 Kang, C.H., Brautigan, D.L., Osherhoff, N. and Margoliash, E., J. Biol. Chem., 253 (1978) 6502–6510.
5 Ermak, D.L. and McCammon, J.A., J. Chem. Phys., 69 (1978) 1352–1360.
6 Turq, P., Lantelme, F. and Friedman, H.L., J. Chem. Phys., 66 (1977) 3039–3044.
7 Fixman, M.J., Chem. Phys., 69 (1978) 1527–1545.
8 Northrup, S.H., Allison, S.A. and McCammon, J.A., J. Chem. Phys., 80 (1984) 1517–1524.
9 Allison, S.A., Northrup, S.H. and McCammon, J.A., J. Chem. Phys., 83 (1985) 2894–2899.
10 Northrup, S.H., Curvin, M., Allison, S.A. and McCammon, J.A., J. Chem. Phys., 84 (1986) 2196–2203.
11 Northrup, S.H., Smith, J.D., Boles, J.O. and Reynold, J.C.L., J. Chem. Phys. 84 (1986) 5536–5544.
12 Ganti, G., McCammon, J.A. and Allison, S.A., J. Phys. Chem., 89 (1985) 3899–3902.
13 Allison, S.A., McCammon, J.A. and Northrup, S.H., In Coulombic Interactions in Macromolecular Systems, ACS Symposium Series, 302, American Chemical Society, Washington, D.C., 1986, pp. 216–231.
14 Allison, S.A., Ganti, G. and McCammon, J.A., Biopolymers, 24 (1985) 1323–1336.
15 Allison, S.A. and McCammon, J.A., J. Phys. Chem., 89 (1985) 1072–1074.
16 Head-Gordon, T. and Brooks III, C.L., J. Phys. Chem., 91 (1987) 3342–3349.
17 Sharp, K., Fine, R., Schulten, K. and Honig, B., J. Phys. Chem., 91 (1987) 3624–3631.
18 Klapper, I., Hagstrom, R., Fine, R., Sharp, K. and Honig, B., Proteins, 1 (1986) 47–59.
19 Allison, S.A., Bacquet, R.J. and McCammon, J.A., preprint.
20 Bernstein, F.C., Koetzle, T.F., Williams, G.J.B., Meyer Jr., E.F., Brice, M.D., Rodgers, J.R., Kennard, O., Shimanouchi, T. and Tasumi, M., J. Mol. Biol., 112 (1977) 535–542.
21 Takano, T. and Dickerson, R.E., Proc. Natl. Acad. Sci. U.S.A., 77 (1980) 6371–6375.
22 Finzel, B.C., Poulos, T.L. and Kraut, J., J. Biol. Chem., 259 (1984) 13027–13036.
23 Matthew, J.B., Ann. Rev. Biophys. Chem., 14 (1985) 387–417.
24 Takano, T., Trus, B.L., Mandel, N., Mandel, G., Kallai, O.B., Swanson, R. and Dickerson, R.E., J. Biol. Chem., 252 (1977) 776–785.
25 Gupta, R.K. and Koenig, S.H., Biochem. Biophys. Res. Commun., 45 (1971) 1134–1143.
26 Moore, G.R. and Williams, R.J.P., Eur. J. Biochem., 103 (1980) 533–541.
27 Warwicker, J. and Watson, H.C., J. Mol. Biol., 157 (1982) 671–679.
28 Pethig, R., Dielectric and Electronic Properties of Biological Materials, Wiley, Chichester, 1979.
29 Warshel, A. and Russell, S.T., Q. Rev. Biophys., 17 (1984) 283–422.
30 Gilson, M.K. and Honig, B.H., Biopolymers, 25 (1986) 2097–2119.
31 Mauk, M.R., Mauk, A.G., Weber, P.C. and Matthew, J.B., Biochemistry 25 (1986) 7085–7091.
32 Poulos, T.L. and Kraut, J., J. Biol. Chem., 255 (1980) 10322–10330.
33 Makinen, M.W., Schichman, S.A., Hill, S.C. and Gray, H.B., Science, 222 (1983) 929–931.
34 Cave, R.J., Sider, P. and Marcus, R.A., J. Phys. Chem., 90 (1986) 1436–1444.
35 Domingue, R.P. and Fayer, M.D., J. Phys. Chem., 90 (1986) 5141–5146.
36 Garcia de la Torre, J., Jimenez, A. and Friere, J., Macromolecules 15 (1982) 148–154.